SVU-International Journal of Engineering Sciences and Applications (2025) 6(1):46-53
Print ISSN: 2785-9967| Online ISSN: 2735-4571
DOI 10.21608/svusrc.2024.319235.1237

Jet Impingement Cooling of Gas Turbine Blade using different configurations of Jet Diameters

M. Khalil [1], Sherif A. Mohamed [1], M. Attalla [2], and Hussein M. Maghrabie[2,]

Abstract: The cooling process of a semi-circular sheet simulating the leading edge of the gas turbine blade has been investigated experimentally in the present study. The circular surface is subjected into five impinging air jets with variable diameter cases at a Reynolds number ranged from 5,000 to 40,000. The diameter of the orifice varies between three configurations namely, Fixed Diameter (FD) case, Ascending Diameter (AD) case, and Descending Diameter (DD) case. The surface temperature has been investigated using Infra-red thermal camera, which provides thermal images of the surface. The results of temperature contours and local heat transfer coefficient have been discussed for the study parameters. The results state that the sides of the sheet that far from impingement get higher temperature while the area beneath the impingement gets higher cooling rates. For FD configuration, the stagnation heat transfer coefficient of the first jet is the highest while the lower case is achieved under the last jet. The stagnation heat transfer coefficient decreases significantly in the flow stream direction for the DD case, and it increases in the case of AD due to the non- uniform impingement flow.

Keywords: Cooling process, Leading edge, Semi-circular sheet, Infra-red thermal camera, Heat transfer coefficient.

1 Introduction

Reducing the amount of cooling fluid in internal cooling channels with improved convective cooling can increase the thermal efficiency of gas turbines. Modern internal cooling systems for gas turbine blades with high thermal loads are made up of several serpentine-shaped cooling channels with angled ribs. Additionally, a great deal of work goes into creating more sophisticated internal cooling configurations with even more improvements to internal heat transfer. Cutting-edge technology may find use in swirl chamber flow configurations, where air passes through a pipe in a swirling motion produced by a tangential jet inlet [1]. It is well known that a gas turbine blade's leading edge has the most important heat transfer area. The leading edge's stagnation zone is where the airfoil's maximum heat transfer rates are consistently found. The creation of more sophisticated internal cooling configurations at the cutting edge is crucial to enhancing the gas turbine thermal efficiency even more. Most blades use a concave channel with multiple inline jets, which is the most advanced leading edge cooling configuration [2-4]. Nevertheless, this type of arrangement also produces a strong spent flow, which weakens the impingement heat transfer and moves the impingement away from the stagnation point [6]. Increasing the airfoil life and overall gas turbine efficiency requires proper and effective cooling of the turbine airfoil leading edge. The leading-edge cavities are frequently roughened on three walls with ribs of various geometries to improve the heat transfer coefficient in those areas [7]. Internal geometrically complex paths are typically used for cooling processes to be matched with the aerodynamic of the blade profile [8].

An innovative internal cooling system has been developed for gas turbines, incorporating dual swirl chambers (DSC) located at the leading edge. This design enhancement aims to address the issue of excessive heat buildup. By utilizing the dual swirl chambers technology, the system can generate two opposing swirls, resulting in a substantial improvement in heat transfer efficiency. A linear impingement effect is produced by the swirl flows' constant reattachment in the center of the chamber during DSC-cooling [9]. The DSC provide better cooling characteristics and better heat transfer uniformity than the traditional direct impingement that is studied by Lin et al [6]. Furthermore,

Received: 8 September 2024; Accepted: 27 November 2024
Corresponding Author: Hussein M. Maghrabie,
E-mail: Hussein_mag@eng.svu.edu.eg, Hussein_mag@yahoo.com
[1] Department of Mechanical Engineering, Faculty of Engineering, Sohag University, P.O. Box 82524, Sohag, Egypt
[2] Department of Mechanical Engineering, Faculty of Engineering, South Valley University, P.O. Box 83523, Qena, Egypt

the DSC cooling configuration exhibits three novel physical phenomena that lead to enhancing heat transfer. The impingement effect has been noted, the fluids in two swirls have experienced increased internal heat exchange; and the cross effect between two chambers has produced a "∞" shaped swirl, which enhances the fluid mixing [10]. Moreover, Mousavi et al. [11] thought that five distinct intake configurations may be used to mimic the swirl chamber (SC) and DSC [12], two distinct chamber types. Moreover, the impact of geometry parameters, such as the aspect ratio of the inlet duct and the merging ratio of the chambers, on the cooling performance has been the focus of additional research on the DSC cooling configuration [10]. Their findings indicated that these geometry parameters affected significantly the pressure drop ratio and heat transfer enhancement.

Kumar and Prasad [13] studied the flow and heat transfer characteristics of circular impinging jets arranged inline normal to a concave surface. The variables were the target plate distance-to-jet diameter ratio, the jet Reynolds number ($\boldsymbol{Re}$), and the inter-jet distance to jet diameter ratio. Moreover, a cylindrical target channel supplied by 10 impinging jets with an axial exit flow at one end of the channel was used to simulate the cooling passage within the leading edge of a turbine blade by Yang et al. [14]. In addition, Liu et al. [15] conducted a numerical simulation to investigate the impingement cooling phenomena occurring in the internal leading-edge region of a high-pressure turbine, predicated on the premise that jet flow is discharged from a configuration of four circular nozzles exhibiting diverse diameters. The findings indicated that the heat transfer coefficient at the leading edge of the turbine blade exhibited an increase correlated with the augmentation of both the jet Reynolds number and the diameters of the jet nozzles. Conversely, the spanwise area-weighted average Nusselt number demonstrated a decline as the ratio of the distance between the jet nozzle and the target surface to the diameter of the jet nozzle intensified. Furthermore, a reduced ratio of the distance between the jet nozzle and the target surface to the jet nozzle diameter was deemed advantageous for optimizing the impingement cooling effect on the leading edge of the turbine blade.

In the present study, the effect of changing impingement flow rate in the stream wise direction will be investigated experimentally. The control of the amount of impingement rate will be conducted using different jet diameters. The principle of increasing and decreasing the jet diameter in stream wise direction has been used for flat plate impingement cooling [16].

The present study employed to apply non-fixed amount of impingement on a semi-circular sheet with a radius of curvature ($\boldsymbol{R}$) of 25 mm by varying the jet diameter. Three different jets diameter configurations namely, Fixed Diameter (FD) jets configuration, Ascending Diameter (AD) jets configuration, and Descending Diameter (DD) jets configurations were examined. The FD case is the regular configuration of the jet diameter where all jets have the same orifice diameter. AD configuration includes orifices with increasing jet diameter in the flow stream direction while DD configuration has a decreasing jet diameter toward the exit direction. The temperature contours and the local heat transfer coefficient on the heated surface will be investigated for the three different diameter configurations at different Reynolds numbers varied from 5,000 to 40,000.

2 Experimental Set-up

Fig. 1 shows the experimental set-up of cooling a semi-circular curved surface simulating the inner surface of gas turbine blade leading edge by a row of five impinging air jets. The apparatus consists of an air compressor with a large storage tank that provides air pressure up to 12 bars to an air pipeline of 12 mm diameter. The pipeline connects the air supply to the plenum chamber including an air dryer, pressure regulator, flow control valve, and digital flow meter. The flow Reynolds number ($\boldsymbol{Re}$) is calculated based on the main pipeline diameter and the mean velocity at the entrance of plenum chamber. The internal dimensions of the plenum chamber are 100 mm width, 200 mm length, and 100 mm height. The bottom side of the plenum chamber, that is 10 mm thick, is perforated with five circular orifices that impinge air into the curved surface.

The curved surface is a 0.3 mm thin sheet made of Inconel material which has electric-thermal properties. The thin sheet is hot rolled to form a semi-circle profile with a 25 mm radius (R) of curvature and a 200 mm length (L) as illustrated in **Fig. 2**. The internal surface of the semi-circular surface will be subjected to the jet flow however the external surface will be exposed to the infra-red camera. The outer surface is painted with a black graphite coat to enhance the precision of the thermal images. During the sheet rolling of the 100 mm side, 10 mm is left straight from both ends for electrical connections. These two straight sides are not painted because of allow electrical elements to directly contacted with Inconel sheet. The Inconel sheet assembled with the plenum by pushing it into a drilled grove as shown in **Fig. 3**. The orifice plate pushes later between the plenum and the Inconel sheet. Thermal grease is used between those moving parts to prevent air leakage through the fittings. The fitting between the moving parts is an interference fit, and more fixation is done after tightening the copper bus bars as will be discussed later.

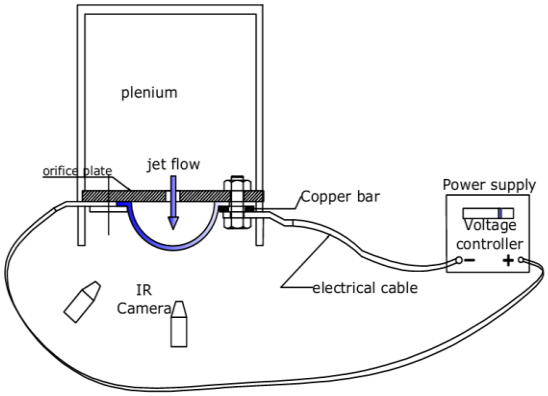

Fig. 1. Experimental setup.

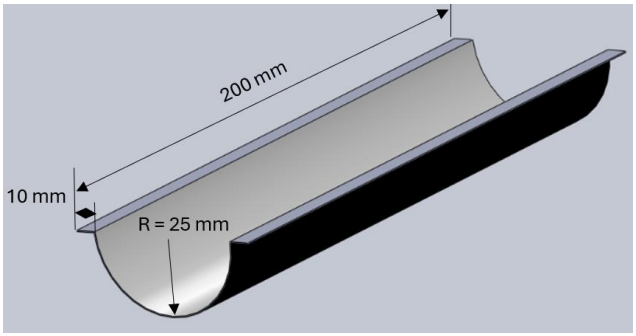

Fig. 2. Semi-circular sheet.

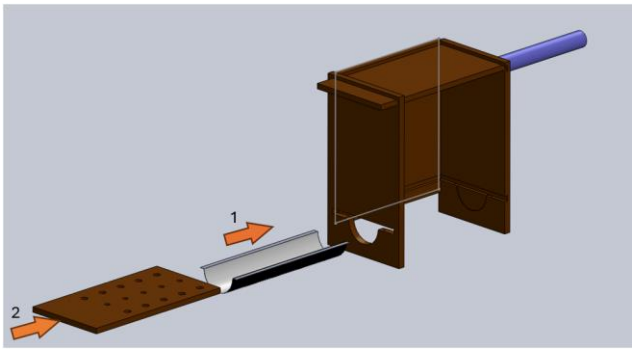

Fig. 3. Installing of the semi-circular sheet with perforated plate and plenum.

The jet-to-jet spacing (***S***) is constant and equals to 30 mm and the jet diameter (***d***) is variable and has three cases of variation. The first case is the fixed diameter jets (FD) in which all jets have the same diameter of $R/d = 4.17$. The second case is ascending diameter jets (AD) in which the jet diameter increases ($\frac{\Delta d_+}{d} = 0.15$) toward the channel exit as shown in **Fig. 4**. The third case is descending diameter jets (DD) in which the diameter decreases ($\frac{\Delta d_-}{d} = 0.15$) in the stream wise direction.

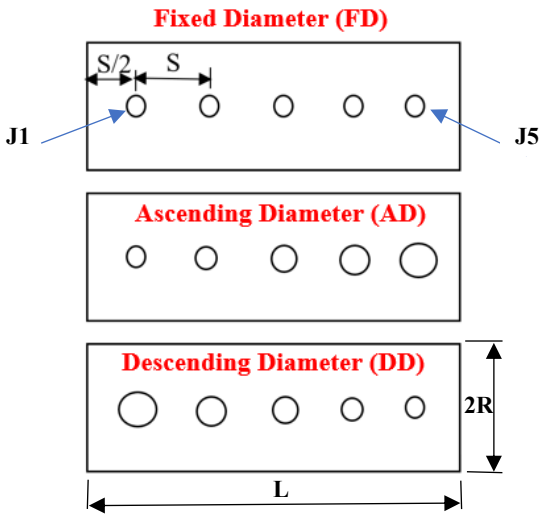

Fig. 4. Specifications of test parameters.

3. Data Reduction

Reynolds number is calculated based on the amount of air mass flow rate at the inlet of the plenum which is measured by the digital flowmeter could be expressed as:

$$Re = \frac{\rho U D}{\mu} = \frac{4\dot{m}}{\pi \mu D} \qquad (1)$$

The semi-circular sheet is made from a metal alloy of Nickel basis Inconel 600 with 200 mm length, 100 mm width, and 0.3 mm thickness. The dimensions of the circular sheet are radius (***R***) and 200 mm length (***L***). The sheet has two straight ends to relate to the electrical supply copper bars as shown in **Fig. 1**. The sheet heated electrically by power supply of 6 V voltage and a current varied from 200 to 300 A to maintain the required heat flux. The copper bars are used to distribute electricity uniformly all over the sheet area. The electrical power from the supply is calculated from:

$$\dot{q}_t = I * V \qquad (2)$$

The electrical heat power supply is dissipated in the form of heat energy due to the property of the sheet material. This heat energy will be absorbed from the heat surface to the atmosphere by forced convection heat transfer of the jet impingement, natural convection around the inner and outer sheet surfaces, conduction heat transfer through the sheet thickness, and radiation heat transfer for both sheet surfaces to the surrounding as follows:

$$\dot{q}_t = \dot{q}_{FC} + \dot{q}_{NC} + \dot{q}_C + \dot{q}_R \qquad (3)$$

According to the collected results from the thermal camera images, the amount of heat transfer by natural convection

and radiation are relatively smaller compared with the forced convection heat transfer so it will be negligible. So, the amount of electrical energy will be dissipated as a convective heat transfer with heat transfer coefficient at any point on the surface (i) and can be calculated as:

$$h_i = \frac{\bar{q}_{FC}}{(T_i - T_\infty)} \qquad (4)$$

The average heat transfer coefficient based on the thermal image of the projected area could be calculated based on the following formula:

$$\bar{h} = \frac{\int \frac{\bar{q}_{FC}}{(T_i - T_\infty)} dA}{\int dA} \qquad (5)$$

To ensure experimental results accuracy, the readings of the thermal camera and the digital flow meter were taken three times with time intervals of ten seconds to maintain a steady state condition. Moreover, the temperature is also calibrated using direct thermocouples which indicate that the difference between the measured value and the calibrated value does not exceed 1%. Uncertainty analysis is conduced of the mass flow rate, surface temperature (T), and the heat transfer coefficient using Kline and McClintock method [17]. The total uncertainties of Re, T, and h are ± 3.80%, ± 1.13%, and ± 1.25%, respectively.

4 Results and Discussion

The experimental results and the main findings of present experimental investigation are presented below using thermal images taken by the Infra-red camera. The image of the projected view to the curved surface is employed to reveal the cooling process of the curved surface. **Fig. 5** represents the temperature contours of the projected curved surface at FD case for different values of Re. For Re = 5,000, the area under the jets is directly affected by the weak impinged flow which is characterized by the small low temperature circles. The sides of the surface are characterized by high temperature color due to the farness from the impingement action. The impingement impact on the surface has an oval area not sharp circle due to the defection of the impinged flow because of the crossflow impact. Increasing Re increases the impinged area and decreases the surface temperature. At Re = 20,000 and 40,000, the impinged areas, that have low temperatures, are merged togethers due to the increase in jet flowrate. The sides are still the hotter area in the whole surface even at high Re. The cold area becomes longitudinal layers in flow stream directions at high Re instead of circles at low values of Re. The sides get the hottest temperature for all cases of Re. It could be summarized that the area under impingement is getting higher heat removal rates relative to the terminals of the sheet.

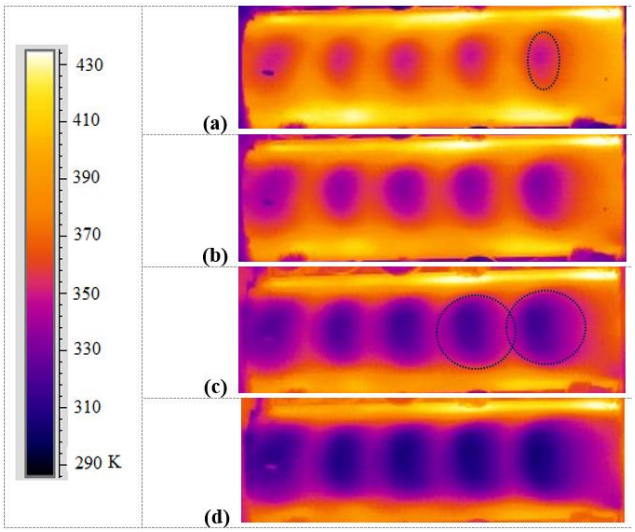

Fig. 5. Temperature contours for FD case at a Re of (a) 5,000, (b) 10,000, (c) 20,000, and (d) 40,000.

Fig. 6 represents the temperature contours for AD case at different values of Re. The increase in orifice diameter interpreted in the low temperature circular area. The first jet (J1) achieves the smallest low temperature circle however the last jet (J5) maintains the largest low temperature circle. The jet impacted area increasingly in its size toward the flow stream exit direction. The temperature trend is repeated for all values of Re while the low temperature area increases with increasing Re. Even at Re = 40,000, the area under the last jet is the greatest area and the area under the first jet is the smallest area. The sides of the surface get better heat transfer rates than those at FD diameter case especially near the surface end where larger diameter jets. Hot spots are generated at the prior of the surface between J1 and J5 at lower Re, e.g., 5,000 and 10,000.

The effect of using DD case on the temperature distribution of the projected surface is presented in **Fig. 7** at different values of Re. The greater orifice diameter is constructed at the frontal part of the channel which enhances impinging more air flow at frontal jets, i.e., J1 and J2. This jet diameter decreases toward the channel exit which leads to decrease the impinged air. The area under the first jet is subjected to a huge amount of air as well as having the maximum cooled circle, temperature of 290 K. The last jet has a very slight impact on cooling the surface beneath due to the small amount of impinged air. Increasing Re increases the area of the cooled circle. The hot spot appears at the lateral part of the surface due to the small diameter in this area, it is about 428 K. The area of the cooled region has a taper shape profile in which the larger cooled area at the beginning of

the channel.

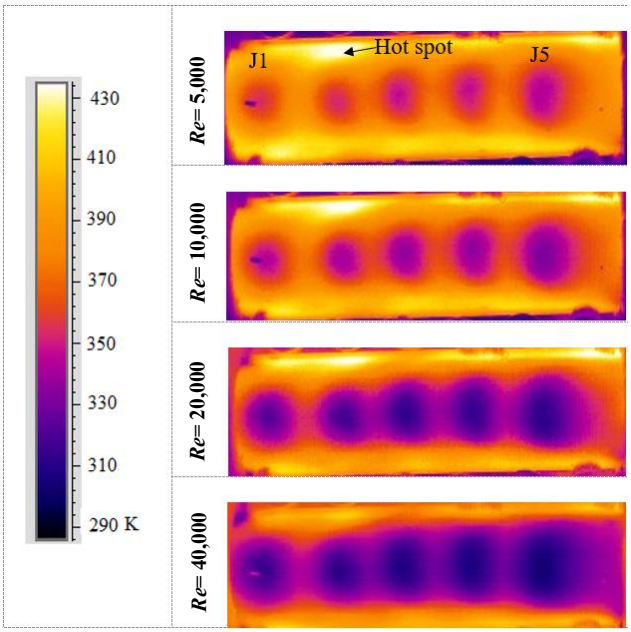

Fig. 6. Temperature contours for AD case at different values of Re.

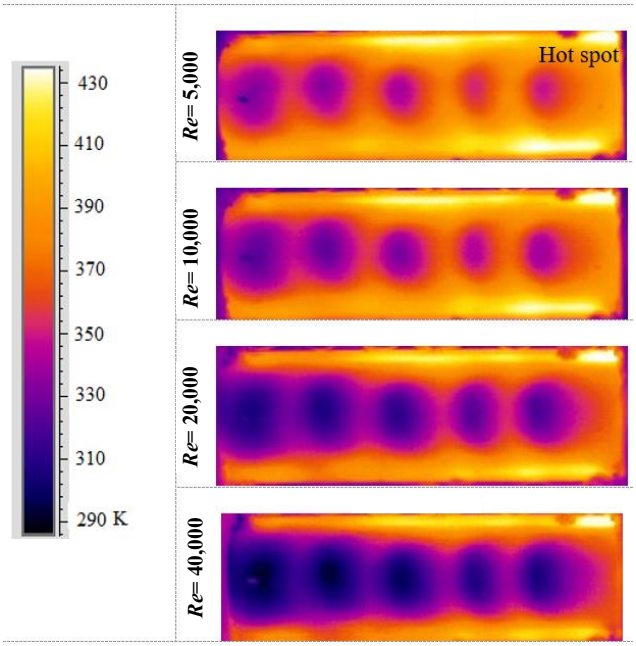

Fig. 7. Temperature contours for DD case at different values of Re.

Fig. 8 represents many different lines constructed on the thermal camera images to investigate the local temperature distribution in different directions for the FD case. Longitudinal line (LL) is constructed stream wise direction at the center of the surface. This LL is used to measure the variation in the surface temperature beneath the jets in the stream wise direction. Ten transverse lines namely, L1, L2, …… L10 are constructed in the transverse directions at the impingement and interaction regions between jets. The point intersecting L1 and LL is located directly beneath the center point of the first jet and the point intersecting L2 and LL is at mid-distance between J1 and J2. The transverse lines are constructed with length equal to $\boldsymbol{S}$.

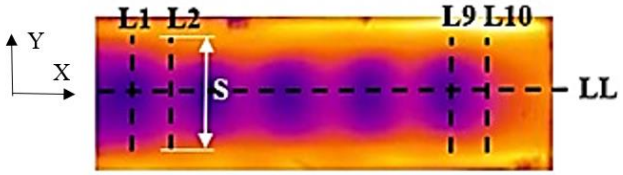

Fig. 8. Temperature contours for FD and Re= 20,000.

The heat transfer distribution in the Y-direction could be illustrated by local heat transfer coefficient on transverse lines L1, L2,…, L10 as shown in **Fig. 8**. In addition, **Fig. 9** represents the local heat transfer coefficient across the transverse lines for different cases of jet diameter at Re of 10,000. For FD case, the distribution of local heat transfer coefficient for all lines has a steep concave shape. Moreover, the five lines under impingement (L1, L3, L5, L7, and L9) have higher values than those at the interaction regions. Moreover, the great variation of h between impingement and interaction lines is at the center line of the jet orifice. This variation decreases away the jet center until it vanishes at a distance of $S/2$ from the jet center. Well, the maximum h is 51 W/m^{2}K which is achieved at the stagnation point of L1; however, the lowest stagnation h is 39 W/m^{2}K that is achieved at L10. For AD case, the profile of local heat transfer coefficient is kept at mild concave shape with a small variation between the impingement and the interaction lines (distribution is convergent). At this configuration, the difference between maximum and minimum stagnation is very slight compared with FD configuration, 50 W/m^{2}K and 46 W/m^{2}K, respectively. The local heat transfer coefficient distribution for DD is characterized with very mild concave shape with small variation between two subsequent lines. However, the difference in the local heat transfer coefficient between L1 and L10 is very significant for the whole distribution domain, it is about 7 W/m^{2}K.

Heat transfer distribution on longitudinal line (LL) for FD case at different values of Reynolds number is presented in **Fig. 10**. The distribution reveals the impact of jet flow on the cooling process where high temperature removal rate is achieved under the jet directly, e.g., the stagnation heat transfer coefficient. At the mid-distance between any two jets, the interaction of jet flow effect has existed where the heat transfer coefficient achieved the lower values [18]. The difference between the maximum and minimum heat transfer coefficient values increases with increasing the Re. At Re = 40,000, this variation is being the significant value. Moreover, the results show that the first jet has the

maximum stagnation heat transfer coefficient, and the last jet has the lower stagnation heat transfer coefficient. The same results trend is achieved at all values of Re while at smaller values of Re the variation of heat transfer distribution is small.

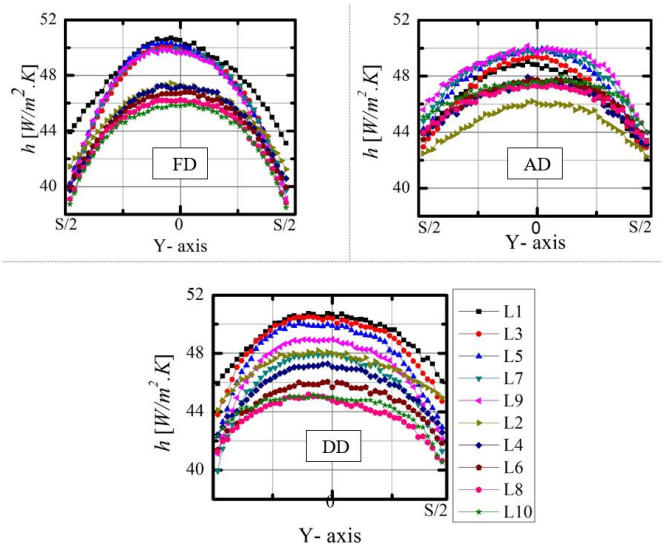

Fig. 9. Local heat transfer coefficient on transverse lines (on Y-axis direction) for all jet diameter cases at Re = 10,000.

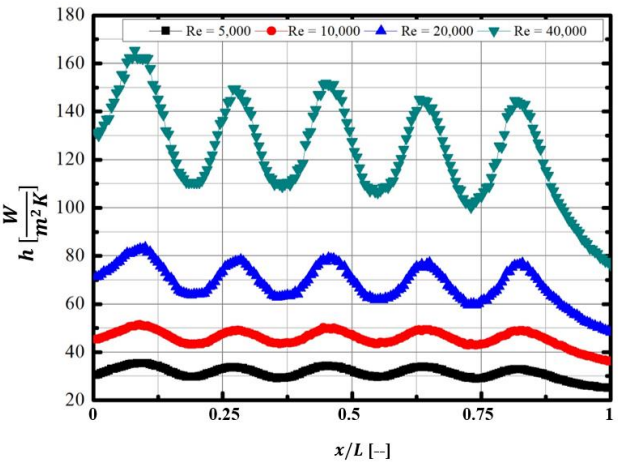

Fig. 10. Local heat transfer coefficient on longitudinal line (LL) for FD case at different values of Re.

The distribution of the local heat transfer coefficient at different diameter cases at Re = 10,000 on LL is presented in **Fig. 11**. For FD, the results trend is discussed previously which state that the first jet has higher stagnation heat transfer coefficient while this stagnation peak decreases in the stream wise direction.

For AD case, where a small amount of jet flow is issued at the first jet that has the lower orifice diameter, the heat transfer coefficient is relatively smaller than those for the lateral jets. The stagnation heat transfer coefficient increases significantly toward the exit direction due to increasing impingement of jet flow because of increasing the jet diameter. The last jet gets the highest stagnation heat transfer while the second jet gets the minimum value. On contrast for DD case where the first jet has the largest diameter, the stagnation heat transfer coefficient decreases in the direction of flow stream. The first jet achieves the maximum stagnation heat transfer coefficient while the last jet achieves the minimum stagnation heat transfer coefficient. Compared with the FD case, the first four jets achieve higher stagnation heat transfer coefficient for DD case than FD case. On the other hand, the first two jets achieve lower stagnation heat transfer coefficient than FD case while the last two jets achieve higher values for AD than the FD case. Moreover, the location of stagnation heat transfer of the last jet for DD case is shifted toward the channel exit due to the deflection of the weak jet flow compare with the CF of the preceding jets [19].

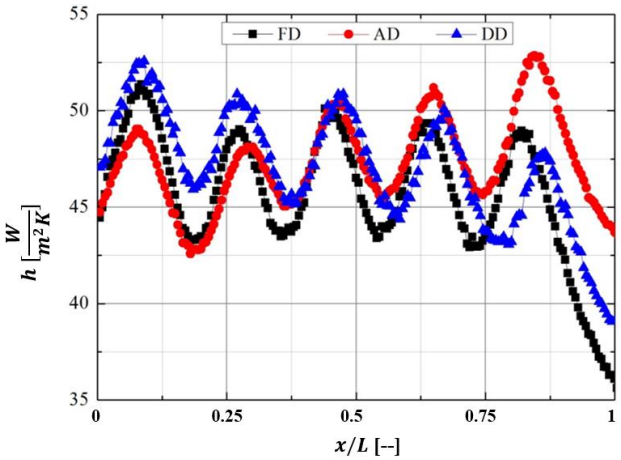

Fig. 11. Local heat transfer coefficient on longitudinal line (LL) for different jet diameter cases at Re = 10,000

The average heat transfer coefficient of the projected thermal image at different diameter cases and different ***Re*** is presented in **Fig. 12.** Increasing ***Re*** increases the average heat transfer coefficient significantly. The increase rate in average heat transfer coefficient decreases while ***Re*** increases. AD case achieved higher $\bar{h}$ comparing with FD and DD case especially at low ***Re***. However, for higher ***Re*** = 25,000 and 30,000, FD and AD cases achieved the same $\bar{h}$. Finally, at low ***Re*** the AD case achieved higher $\bar{h}$ however, the FD case achieved higher $\bar{h}$ at high ***Re***.

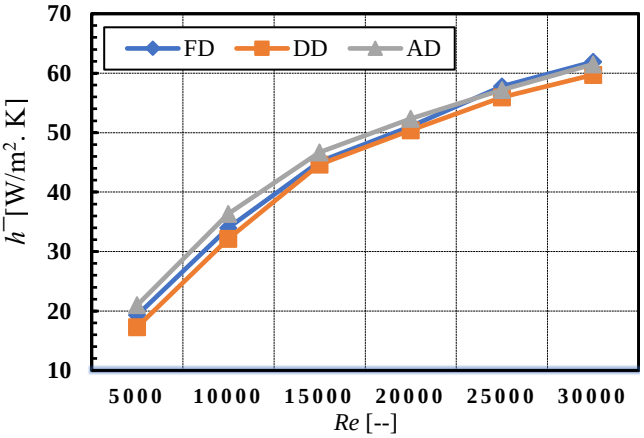

Fig. 12. Average heat transfer coefficient of the projected thermal image for all jet diameter cases at different ***Re***.

5. Conclusions and Recommendations

Experimental study of using variable jet diameter for cooling a semi-circular sheet simulating the leading edge of turbine blade has been conducted in the current implementaion. The effect of using jets diameter configurations and Reynolds number on the heat transfer distribution of the semi-circle are investigated. The main significant results of the study are:

- The area under impingement has higher heat removal rates relative to the terminals of the sheet.
- The peak of the heat transfer coefficient is achieved under the jet directly which is called stagnation point while the lower heat transfer coefficient is achieved at the interaction point between each two jets.
- The maximum stagnaion heat transfer coefficient is 51 W/m^{2}K at L1 for the FD configuration while the minimum stagnation stagnaion heat transfer coefficient is 45 W/m^{2}K at L10 for the DD configuration.
- The AD diameter configuration enhances the heat removal rates near the end of the surface while the DD configuration enhances it at the front of the surface with respect to the exit direction.
- The analysis of the average heat transfer coffecient concluding that at low Re the AD case achieved higher $\bar{h}$ however, FD case achieved higher $\bar{h}$ at high Re.

Finally, the study explains that the AD configuration enhances the heat transfer rates and enhances strongly the heat transfer distribution for multiple jet impingement issues.

References

[1] M. K. Karsten Kusterer, Gang Lin, Dieter Bohn, Takao Sugimoto, Ryozo Tanaka, "Heat transfer enhancement for gas turbine internal cooling by application of double swirl cooling chambers," in *Proceedings of ASME Turbo Expo 2013: Turbine Technical Conference and Exposition*, 2013, pp. 1–11.

[2] Z. Ying, L. Guiping, B. Xueqin, B. Lizhan, and W. Dongsheng, "Experimental study of curvature effects on jet impingement heat transfer on concave surfaces," *Chinese J. Aeronaut.*, vol. 30, no. 2, pp. 586–594, 2017, doi: 10.1016/j.cja.2016.12.032.

[3] H. Xing, W. Du, P. Sun, S. Xu, D. He, and L. Luo, "Influence of surface curvature and jet-to-surface spacing on heat transfer of impingement cooled turbine leading edge with crossflow and dimple," I*nt. Commun. Heat Mass Transf.*, vol. 135, no. June, pp. 931–943, 2022, doi: 10.1016/j.icheatmasstransfer.2022.106116.

[4] J. Li, B. Yu, X. Li, S. Bu, and A. Wang, "Multi-jet impingement cooling in the leading edge of turbine blade using matrix as internal structure," *Appl. Therm. Eng.*, vol. 250, no. May, p. 123531, 2024, doi: 10.1016/j.applthermaleng.2024.123531.

[5] M. Fenot, E. Dorignac, and J. Vullierme, "An experimental study on hot round jets impinging a concave surface," *Int. J. Heat Fluid Flow*, vol. 29, pp. 945–956, 2008, doi: 10.1016/j.ijheatfluidflow.2008.03.015.

[6] G. Lin *et al.*, "Numerical investigation on heat transfer in an advanced new leading edge impingement cooling configuration," *Propuls. Power Res.*, vol. 4, no. 4, pp. 179–189, 2015, doi: 10.1016/j.jppr.2015.10.003.

[7] M. E. Taslim and L. Setayeshgar, "Experimental Leading-Edge Impingement Cooling Through Racetrack Crossover Holes," *ASME Turbo Expo, 2001-GT-0153*, pp. 1–9, 2001, doi: 10.1115/2001-GT-0153.

[8] K. Elebiary and M. E. Taslim, "Experimental/Numerical Crossover Jet Impingement in an Airfoil Leading-Edge Cooling Channel," *J. Turbomachinery,ASME*, vol. 135, no. 5, p. 011037, 2013, doi: 10.1115/1.4006420.

[9] H. M. Maghrabie, "Heat transfer intensification of jet impingement using exciting jets - A comprehensive review," Renew. Sustain. Energy Rev., vol. 139, p. 110684, 2021, doi: 10.1016/j.rser.2020.110684.

[10] G. Lin, K. Kusterer, D. Bohn, T. Sugimoto, R. Tanaka, and M. Kazari, "Investigation on heat transfer enhancement and pressure loss of double swirl chambers cooling," *Propuls. Power Res.*, vol. 2, no. 3, pp. 177–187, 2013, doi: 10.1016/j.jppr.2013.07.003.

[11] S. M. Mousavi, B. Ghadimi, and F. Kowsary, "Numerical study on the effects of multiple inlet slot configurations on swirl cooling of a gas turbine blade leading edge," *Int. Commun. Heat Mass Transf.*, vol. 90, pp. 34–43, 2018, doi: 10.1016/j.icheatmasstransfer.2017.10.012.

[12] X. Fan, "Numerical research of a new vortex double wall cooling configuration for gas turbine blade leading edge," *Int. J. Heat Mass Transf.*, vol. 183, no. February, pp. 133–149, 2022, doi: 10.1016/j.ijheatmasstransfer.2021.122048.

[13] B. V. N. R. Kumar and B. V. S. S. S. Prasad, "Computational flow and heat transfer of a row of circular jets impinging on a concave surface," *Heat Mass Transf.*, vol. 44, no. 6, pp. 667–678, 2008, doi: 10.1007/s00231-007-0274-3.

[14] L. Yang, J. Ren, H. Jiang, and P. Ligrani, "Experimental and numerical investigation of unsteady impingement cooling within a blade leading edge passage," *Int. J. Heat Mass Transf.*, vol. 71, pp. 57–68, 2014, doi: 10.1016/j.ijheatmasstransfer.2013.12.006.

[15] Z. Liu, Z. Feng, and L. Song, "Numerical Study of Flow

and Heat Transfer of Impingement Cooling on Model of Turbine blade Leading Edge," in *Proceedings of ASME Turbo Expo 2010*, 2010.

[16] Y. Ji, P. Singh, S. V. Ekkad, and S. Zang, "Effect of crossflow regulation by varying jet diameters in streamwise direction on jet impingement heat transfer under maximum crossflow condition," *Numer. Heat Transf. Part A Appl.*, vol. 72, no. 8, pp. 579–591, 2017, doi: 10.1080/10407782.2017.1394136.

[17] J. P. Holman, Experimental Methods for Engineers, eighth ed., New York, United States: McGraw-Hill Series, 2012.

[18] W. Wu, R. Yao, J. Wang, H. Su, and X. Wu, "Leading edge impingement cooling analysis with separators of a real gas turbine blade," *Appl. Therm. Eng.*, vol. 208, no. May, 2022, doi: 10.1016/j.applthermaleng.2022.118275.

[19] M. Khalil, S. A. Mohamed, M. Attalla, and H. M. Maghrabie, "Cooling of Gas Turbine Blade Leading Edge Via an Array of Air Jets With Variable Diameters," *J. Heat Transfer*, vol. 144, no. 12, p. 123801, Dec. 2022, doi: 10.1115/1.4055598.

Nomenclature	
D	plenum inlet diameter [m]
d	orifice diameter [m]
$\Delta \boldsymbol{d}$	diameter increment/decrement[m]
h	heat transfer coefficient [W/m^2.K]
I	electrical current [A]
L	channel length [m]
$\dot{m}$	mass flow rate [kg/s]
$\bar{q}$	heat flux [W/m^2]
$\dot{q}$	heat generation [W]
R	curved surface radius
Re	Reynold s number [--]
S	jet-to-jet spacing [m]
T	temperature [K]
V	voltage [V]
Greek symbols	
μ	dynamic viscosity [kg/m .s]
P	density [kg/m^3]
Subscripts	
C	Conduction heat transfer
FC	Forced convection
I	Location annotation
NC	Natural convection
R	Radiation heat transfer
T	total
∞	ambient
+	increase
-	decrease
Acronyms	
AD	Ascending diameter jets
DD	Descending diameter jets
DSC	Double swirl chamber
FD	Fixed diameter
IR	Infra-red
L	Transverse Line
LL	Longitudinal Line
J	Jet
SC	Single Swirl Chamber